Nuclear Science and Techniques (2026) 37:12
https://doi.org/10.1007/s41365-025-01825-x

Efficient control and removal of laser-generated aerosol particles by combining water spray with pre-injection of electrical charged mist for nuclear reactor decommissioning

Ruicong Xu[1,2] · Avadhesh Kumar Sharma[3] · Zeeshan Ahmed[1] · Ravinder Kumar[1] · Laffolley Hugo[4] · Ryo Yokoyama[1,2] · Shuichiro Miwa[1,2] · Shunichi Suzuki[5] · Atsushi Kosuge[6]

Received: 12 May 2025 / Revised: 13 June 2025 / Accepted: 19 June 2025 / Published online: 7 December 2025

Abstract
Laser-induced aerosols, predominantly submicron in size, pose significant environmental and health risks during the decommissioning of nuclear reactors. This study experimentally investigated the removal of laser-generated aerosol particles using a water spray system integrated with an innovative system for pre-injecting electrically charged mist in our facility. To simulate aerosol generation in reactor decommissioning, a high-power laser was used to irradiate various materials (including stainless steel, carbon steel, and concrete), generating aerosol particles that were agglomerated with injected water mist and subsequently scavenged by water spray. Experimental results demonstrate enhanced aerosol removal via aerosol-mist agglomeration, with charged mist significantly improving particle capture by increasing wettability and size. The average improvements for the stainless steel, carbon steel, and concrete were 40%, 44%, and 21%, respectively. The results of experiments using charged mist with different polarities (both positive and negative) and different surface coatings reveal that the dominant polarity of aerosols varies with the irradiated materials, influenced by their crystal structure and electron emission properties. Notably, surface coatings such as ZrO_2 and CeO_2 were found to possibly alter aerosol charging characteristics, thereby affecting aerosol removal efficiency with charged mist configurations. The innovative aerosol-mist agglomeration approach shows promise in mitigating radiation exposure, ensuring environmental safety, and reducing contaminated water during reactor dismantling. This study contributes critical knowledge for the development of advanced aerosol management strategies for nuclear reactor decommissioning. The understanding obtained in this work is also expected to be useful for various environmental and chemical engineering applications such as gas decontamination, air purification, and pollution control.

Keywords Laser-induced aerosol generation · Aerosol removal · Electrically charging mist · Agglomeration · Water spray scavenging · Reactor decommissioning

1 Introduction

In many industrial activities, harmful submicron- and micron-sized aerosol particles are generally generated using effluent gases [1]. During various chemical and nuclear engineering processes, the release of these aerosols into the environment presents notable ecological and public health challenges, as they can penetrate deeply into the human pulmonary system and lead to the development of various diseases by inhalation [2]. Typically, aerosol production during the decommissioning and dismantling of nuclear reactors raises critical concerns owing to its potential risks to workers and environmental radiation exposure [3–5]. The management and removal of aerosol particles is vital because of their implications for occupational safety and environmental integrity [6, 7]. Moreover, the generation of radioactive aerosols should be further considered in the context of dismantling nuclear reactors after severe accidents. For example, the decommissioning of Fukushima Daiichi nuclear reactors, which is a global challenge for the future of nuclear energy and environmental protection, necessitates

The authors appreciate the financial support from the Nuclear Energy Science & Technology and Human Resource Development Project of the Japan Atomic Energy Agency/Collaborative Laboratories for Advanced Decommissioning Science (No. R04I034). The author Ruicong Xu appreciates the scholarship (financial support) from the China Scholarship Council (CSC, No. 202106380073).

Extended author information available on the last page of the article

the use of advanced remote techniques, such as high-power laser irradiation, for containment cleaning and fuel debris retrieval under complex operational conditions [8, 9].

Compared with mechanical approaches, high-power fiber lasers demonstrate exceptional capabilities in achieving minimal material removal, generating a reduced mass of re-suspended aerosols, effectively cutting high-hardness materials (such as fuel debris), and offering high-precision, non-contact operation and suitability for accessing locations requiring extended working distances. [9–11]. However, laser irradiation is expected to generate smaller-sized radioactive aerosol particles, which are generally submicron in size [3, 11–15]. The dispersion and deposition of these radioactive aerosols within the primary containment vessel and surrounding structures could pose a significant radiological hazard to the public and environment [13–17]. Thus, it is crucial to manage and eliminate these radioactive aerosols within the reactor primary containment vessel to prevent the release of radioactivity into the environment, reduce harmful impacts on humans and wildlife from increased radiation exposure via inhalation, and diminish radioactive contamination of the soil.

To facilitate the safe dismantling of reactors and mitigate the environmental release of radioactive materials, containment water spray systems are utilized for aerosol removal with several notable benefits, including the cooling of high-temperature fuel debris with decay heat and reduction of fire hazards [18, 19]. As illustrated in Fig. 1a, sprayed water droplets effectively capture aerosol particles through various mechanisms, including mechanical (e.g., Brownian diffusion, inertial impaction, and interception), phoretic (e.g., diffusio- and thermophoresis), and electrostatic processes. Experimental frameworks have been established to investigate aerosol dynamics such as deposition and spray removal under diverse conditions in nuclear facilities. Examples include deposition studies conducted at the National Aerosol Test Facility (NATF) facility [20], Filtered Containment Venting Systems (FCVS) [21], and our long-pipe system [22]. Additional spray removal experiments have been performed in different facilities, such as TOSQAN (TOnus Qualification ANalytique) [18, 23], SCRUPOS (SCRUbbing by Pool and Spray) [24], COSTTHES (Containment Source Term and Thermal Hydraulics Experiment System) [25], THAI (thermal-hydraulics, hydrogen, aerosols, and iodine) [19, 26], and our UTARTS (University of Tokyo, Aerosol Removal Tests using Sprays) facilities [27–33].

However, as confirmed by previous spray removal studies [13, 14, 18, 19, 24–36], it was noted that aerosol particles with greenfield-gap sizes (i.e., diameter within 0.1 ~ 1 μm) are difficult to remove by spray droplets [4, 37, 38]. Unfortunately, a larger fraction of aerosol particles is expected to be generated when applying laser techniques for nuclear reactor decommissioning [3, 13, 14, 30, 32, 39]. Enhancing the

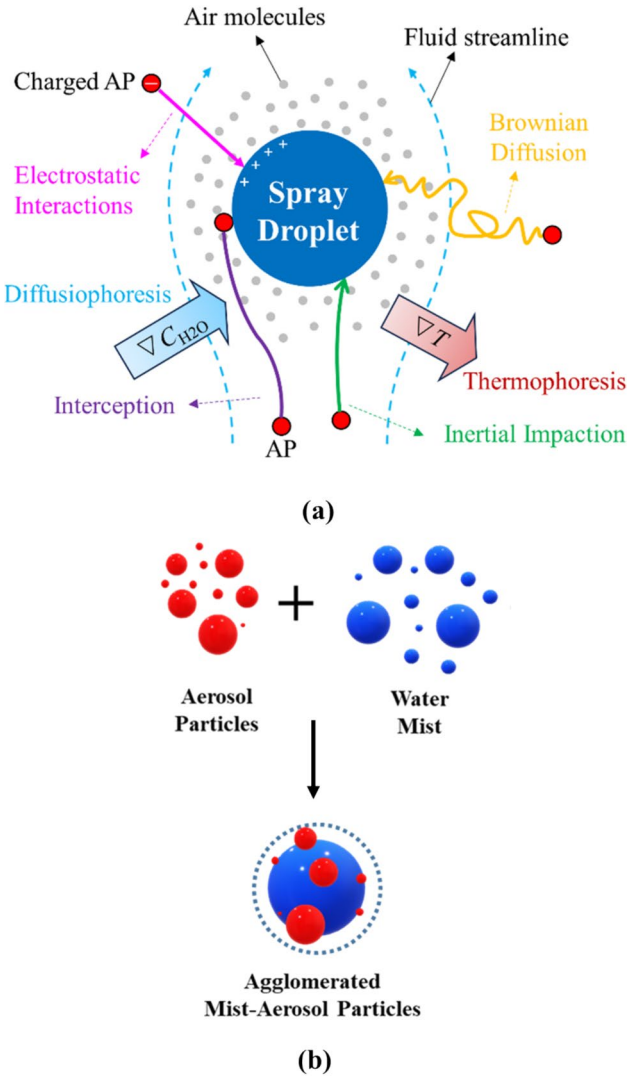

Fig. 1 (Color online) Illustrations of: **a** mechanisms for sprayed water droplets to capture aerosol particles, **b** agglomeration of water mist and aerosol particles to enlarge particle sizes [31]

aerosol scavenging efficiency through electrical charging of the spray has shown significant potential applicability. Coulombic interactions between charged droplets and aerosols substantially improve the particle capture [30, 40]. Many investigations emphasize the need to optimize charging system configurations, including charging methods, electrode geometry, placement, and voltage characteristics [41–46]. Different charging approaches, such as induction, conduction, and corona discharge, exhibit varying efficiencies under specific operating conditions [47]. Parameters such as the voltage settings and electrode configurations significantly influence the electric fields produced by these systems [41, 44, 45, 48]. Recent experiments conducted at our UTARTS facility highlighted the effectiveness of improved induction

electrode designs for enhancing the aerosol scavenging performance [48].

However, the removal efficiency of aerosols can be improved by agglomeration methods such as chemical [49], acoustic [50, 51], and electrostatic methods [52]. Agglomerated particles with larger sizes can be more easily captured by droplets through enhanced mechanical effects. However, the implementation of these methods in the context of damaged reactor dismantling is restricted by harsh operational conditions including intense radiation exposure. For instance, chemical and acoustic agglomerations face limitations owing to their associated environmental pollution and high energy requirements. In contrast, electrostatic agglomeration using AC voltage, as suggested by Watanabe et al. [52], appears to have broader potential for industrial applications. Despite this, integrating electrostatic precipitators with surface cleaning and debris-cutting technologies (e.g., mechanical or laser systems) into high-radiation environments characterized by complex thermal–hydraulic interactions and multiscale phenomena remains a formidable challenge. To address these limitations, in recent years, we introduced an innovative agglomeration strategy that involves the pre-injection of submicron water mist particles prior to spray activation. As shown in Fig. 2(b), this method promotes aerosol-mist agglomeration, thereby increasing the particle size and enhancing the particle wettability. Water mist interacts with aerosols through various mechanisms, including Brownian motion, gravitational settling, laminar and turbulent shear, turbulent inertial coagulation, and shear-induced coagulation [53–57]. Experimental investigations conducted at UTARTS demonstrated that pre-injecting water mist substantially enhances aerosol scavenging efficiency [27–32, 48, 58–60]. However, the studies also revealed that the effectiveness of this approach is influenced by the operational characteristics of the spray, particularly the droplet velocity [31]. Recently, we developed an electrostatic

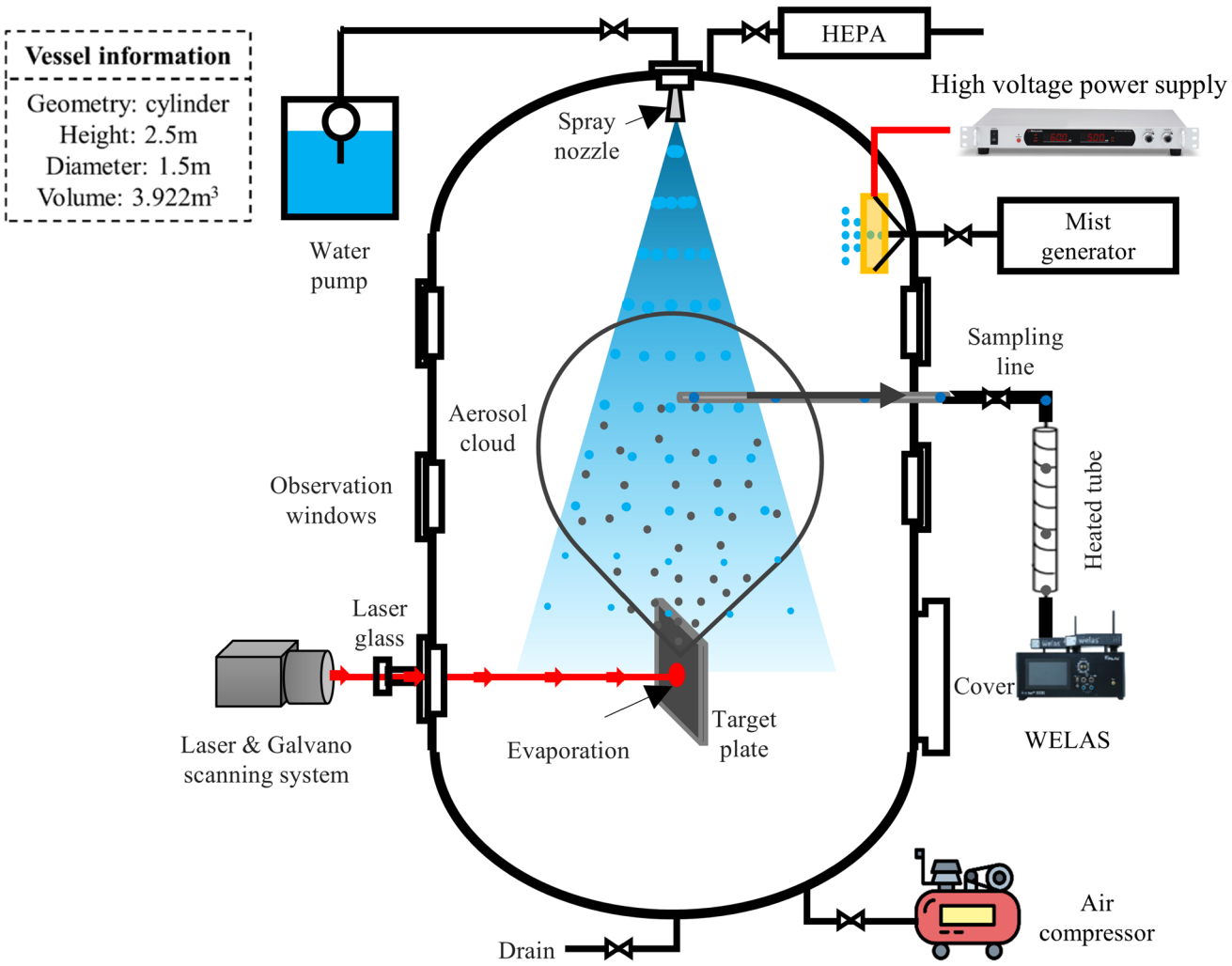

Fig. 2 (Color online) Schematic of UTARTS facility for laser-induced aerosol generation and spray scavenging experiments

charging system for water mist during their injection [59]. The charged water mist is supposed to enhance the aerosol-mist agglomeration. Using zirconia aerosol particles as simulant aerosols generated from laser irradiation, we validated the effectiveness of charging mist in accelerating aerosol removal.

Effective aerosol management and mitigation are of great importance for reducing radiation exposure and minimizing contaminated water production in damaged reactor dismantling. Many previous investigations have provided valuable insights into the characterization of laser-induced aerosols and improved aerosol removal by spray scavenging. However, the techniques for improving aerosol removal have mostly been verified using simulant aerosols. Our study aimed to develop efficient methods and strategies for controlling aerosol dispersion during laser cutting and decontamination processes and to mitigate radiation risks. Therefore, the applicability of these developing techniques must be validated in a more realistic scenario, which is of great significance for the technical strategies of reactor dismantling and decommissioning.

To explore more realistic conditions for Fukushima Daiichi decommissioning, in this study, innovative experimental studies are performed in our UTARTS facility for the removal of aerosols generated from laser irradiation by water sprays by improving the electrical charging mist system. The primary objective was to adapt our techniques for remote dismantling activities at the Fukushima Daiichi nuclear reactor and to address radiation hotspots. This study offers important knowledge and potential applications for the decontamination and prevention of fine particle dispersion, ensuring environmental safety, and prolonging the operational lifespan of electronic equipment. Furthermore, insights gained from this study can be useful for surface cleaning and the destruction of structures or buildings contaminated by hazardous substances, ensuring compliance with safety standards set by relevant industries.

2 Experimental conditions

2.1 Basic experimental setup

Figure 2 illustrates a schematic of the UTARTS facility for our laser-induced aerosol generation and spray scavenging experiments with pre-injection of charged water mist. The UTARTS facility was designed to replicate various phenomena, including laser decontamination and concurrent mist and spray operations. Its main containment vessel, constructed from stainless steel, has a height of 2.5 m, diameter of 1.5 m, and total volume of 3.92 m^3. The vessel was equipped with 13 optical windows positioned along the sidewalls for internal observation and measurement. A single access manhole was integrated into the wall to facilitate post-experimental cleaning. Several pipes were installed within the vessel for aerosol and mist injections, aerosol sampling, and data collection. The aerosol sampling lines were connected to aerosol analyzers Palas Welas 3000, which are capable of measuring submicron aerosol particles. A 1.5-kW continuous-wave (CW) fiber laser with a Galvano scanning system was employed for laser irradiation. Test surfaces made of materials such as carbon steel (CS), stainless steel (SS), and concrete were subjected to infrared (IR) laser irradiation at varying power levels. Gas and water discharge pipes equipped with valves at the top and bottom of the vessel allowed for the removal of aerosol particles and water after the experiments. Before the release, the gas was filtered through a High-Efficiency Particulate Air (HEPA) filter. An air compressor was used to inject dry air into the vessel, ensuring a uniform distribution of aerosol particles (generally, a 5-min dry air injection was adopted, as confirmed by our previous experiments measuring aerosol concentration at varying locations in the facility [31]). A spray system installed at the top center of the vessel features a nozzle for injecting water droplets to capture aerosol particles. Additionally, the mist injection and charging systems were mounted on the side wall to introduce water mist into the vessel, further facilitating aerosol particle management.

2.2 Laser light source and Galvano scanning system

A Class-4 continuous oscillation fiber laser (Raycus, RFL-C1500) with a maximum output power of 1.5 kW and central wavelength of 1080 nm served as the laser light source for processing. The system was managed by a digital controller, NCL-151 (NISHIHARA), which also supported a maximum output of 1.5 kW. A Galvano scanning system was integrated into the laser head to enable precise scanning of the designated areas on the irradiated specimen surface. The Galvano scanning system comprises a laser, galvanometers (a set of mirrors), and lenses that focus the laser beam onto the target location. This setup provides a highly effective solution for laser-scanning applications, offering precision and versatility for tasks such as laser cleaning, cutting, and welding. The galvanometers were mounted on high-speed motors to ensure rapid and accurate movement, with their positions controlled electronically. The Galvano scanning system featured a focal length of 900 mm and an effective focal length of 998 mm. The lenses used in the scanner are typically crafted from high-quality materials, such as quartz or sapphire, to minimize the heat generation from the laser and ensure optimal performance. In this study, the laser power was fixed at 1.5 kW for the larger amount of aerosol particles generated.

2.3 Test specimens

The materials selected for the laser cleaning experiments included various surfaces of CS (grade SS400), SS (grade SS304), and concrete, chosen for their widespread use in numerous industrial applications, particularly in nuclear reactor pressure vessels and containment vessels. These materials exhibit distinct thermophysical properties that influence the laser cleaning efficiency. Additionally, different coatings were applied to these base materials to evaluate the effectiveness of laser cleaning on the coated surfaces. ZrO_2 and CeO_2 were used as coatings to simulate the nuclear decommissioning conditions [15]. The coating solution was prepared by mixing distilled water and nanoparticles in a 50:50 ratio, followed by sonication using an Ultrasonic Sonicator for 60 min to ensure uniform dispersion. The solution was applied to the specimen surfaces using a spray gun with three successive applications to achieve consistent coating coverage. This study aimed to assess the potential of laser cleaning for removing contaminants from coated surfaces and the applicability of advanced agglomeration techniques to subsequent aerosol spray scavenging. The selection of materials for the specimens and coatings reflects the practical demands of decommissioning applications, providing a thorough evaluation of the effectiveness of laser cleaning on diverse surface types and coatings.

2.4 Water spray system

As shown in Fig. 2, the spray system was installed at the top center of the vessel, featuring a nozzle for injecting water droplets to capture aerosol particles. The spray water flow rate was regulated at 2 L/min using a pump in current experiments. In this study, a single-hole full-cone nozzle (model: 1/8 GG-SS3004) fabricated by Spraying System Co. was used. Spray droplet characterization was performed in our previous studies [28, 29]. Table 1 lists the parameters of the nozzle and sprayed droplets in the current study. Figure 3a and b illustrates the size distribution of the droplets generated under 2 L/min spraying and the flow pattern inside the vessel during spraying.

Table 1 Parameters of the spray nozzle [31]

Model	1/8 GG-SS3004
Orifice diameter (mm)	1.2
Spray angle[a] (°)	26–32
Droplet velocity magnitude at 2 L/min[b] (m/s)	20
Droplet Sauter mean diameter (μm)	309
Spray pattern of the nozzle	Full cone
Distance from the top of vessel (h_{Nozzle}) (mm)	300
Water pressure for 2 L/min spray (MPa)	0.53

[a]The data were given by the manufacturer

[b]The droplet velocity were measured near the nozzle outlet by using the PIV (Particle Image Velocimetry) [27]

2.5 Mist generation and charging systems

The water mist injection system was designed to horizontally introduce submicron water mist particles into the UTARTS facility from its sidewall. An ultrasonic mist generator (MZ-JH30, Yamazen Company, Japan) capable of producing varying levels of mist concentrations was employed for this purpose. As illustrated in Fig. 4, the size distributions of water mist particles at the lowest and highest mist concentration levels (C_{mist}) generated by the system were relatively consistent. Regardless of the concentration level, the water mist particle sizes were predominantly centered around 0.68 μm. The water mist particles are also in the submicron range.

According to the spray charging methods (e.g., induction, conduction, corona discharge) that have been widely applied in many industrial fields [61, 62], several methods might be applicable for charging water mist. Induction and conduction are the primary methods used to charge conducting liquids [63]. In induction charging, an electric charge is applied to droplets after atomization, whereas conduction charging involves transferring an electric charge to a liquid jet and its resulting droplets by directly connecting the atomizer nozzle to a high-voltage source. Although the droplets can also be charged after atomization, for example by gaseous ions generated by corona discharge, their charge is much lower than that produced by the other two methods. Both methods can achieve comparable charge levels for droplets [46]. However, in the context of this study, the water mist to be charged consists of much smaller particles (primarily submicron in size) than spray droplets, which typically range from tens to several hundred microns. In addition, the atomization process for generating water mist occurred within the mist generator. Given these characteristics, the induction charging method is more suitable for charging mist in this setup.

Figure 5 shows the mist charging system used in this study. To charge the water mist, a cylindrical brass electrode, which was confirmed as the optimal electrode in our previous study [59], was installed at the outlet of the mist injection pipe inside the vessel. This electrode was connected to a high-voltage power supply (Matsusada Precision, HAR-30R10), which can provide an adjustable charging voltage and polarity (positive or negative). The mist injection pipe, made of stainless steel, was grounded to establish an electric field near the pipe outlet, facilitating the electrical charging of the water mist.

2.6 Aerosol sampling and measurement system

For aerosol measurements, we installed a sampling line above the laser target. During the measurements, aerosol

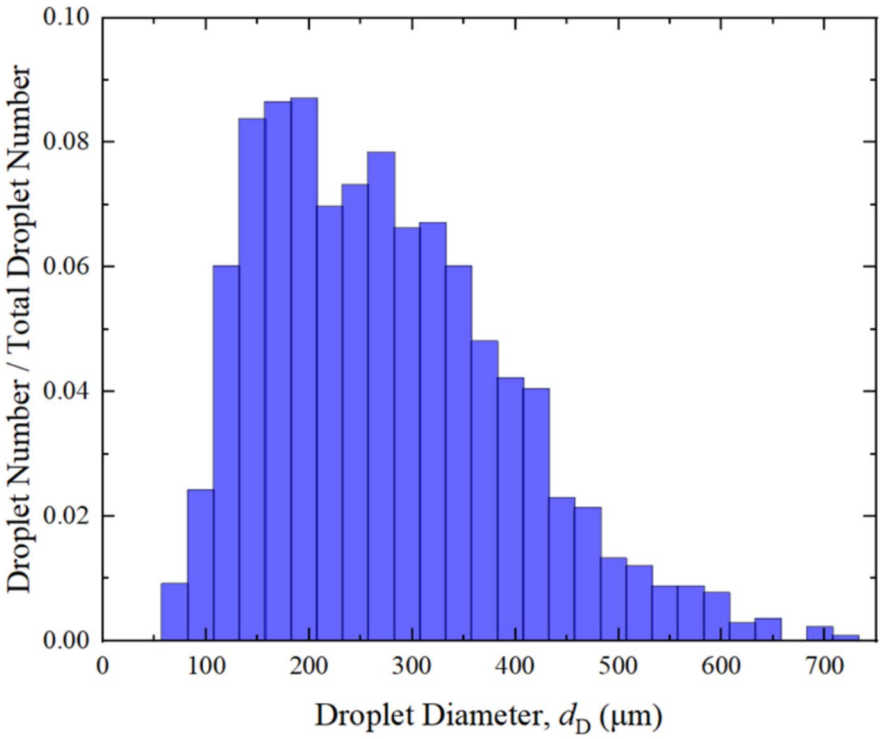

(a)

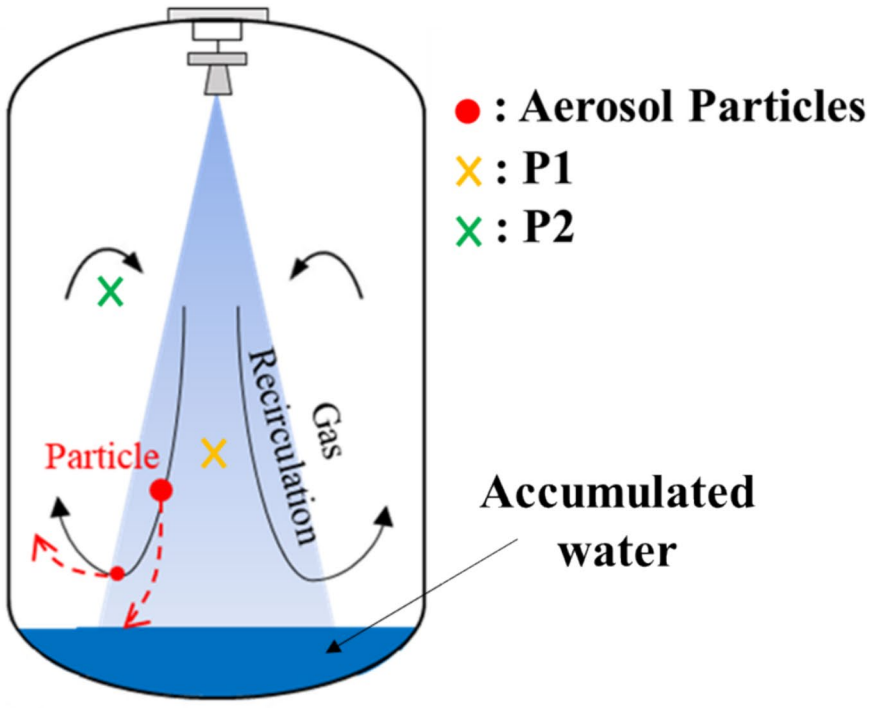

(b)

Fig. 3 (Color online) Characteristics of water spray system: **a** droplet size distribution at 2 L/min spray [27]; **b** flow pattern inside the vessel

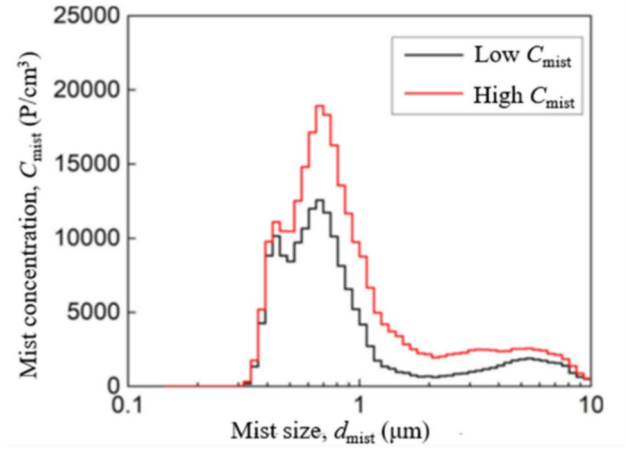

Fig. 4 Size distributions of injected water mist [27]

particle-laden gas was sampled to evaluate variations in aerosol concentrations. Based on prior uncertainty analyses [29, 30], the sampling efficiency for submicron aerosol particles in this experimental system exceeded 90%. To remove water mist from the sampling flows before they entered the aerosol analyzer, a heater-wrapped tube with a fixed temperature and of 1.2 m in length was installed upstream of the analyzer. After passing through the heated tubes, the aerosol sample flows were directed into a Palas Welas 3000 aerosol analyzer, which measured the aerosol particle number concentration (C_n) and size distribution during the experiments. The detailed specifications of Palas Welas 3000 are listed in Table 2. Concurrently, time-resolved measurements of temperature, humidity, pressure, and spray flow rate were conducted along with aerosol analysis. Table 3 summarizes

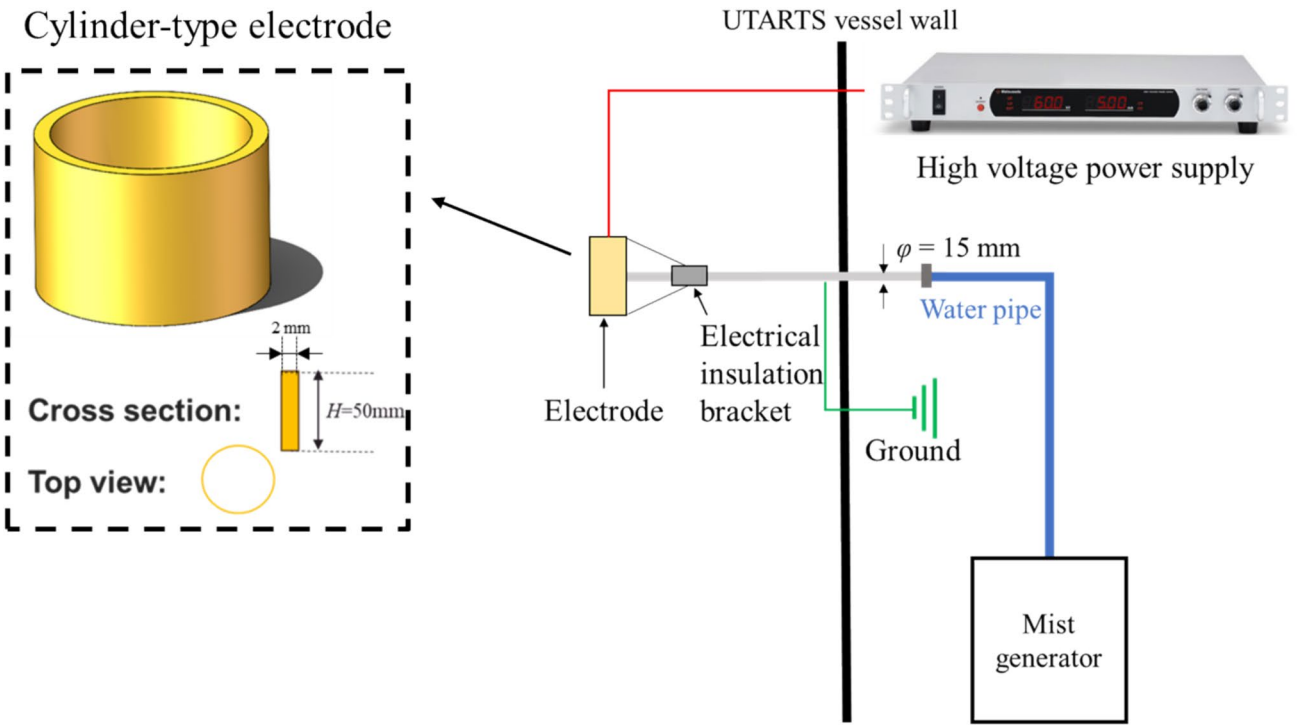

Fig. 5 (Color online) Schematical illustration of mist charging system

Table 2 Specifications for aerosol analyzer WELAS 3000 [30]

Working principle	Light-scattering spectrometer
Particle type	Solid, liquid
Measurement range for aerosol diameter (μm)	0.2 ~ 10
Absolute measurement error (μm)	0.01
Relative measurement error	5%
Number concentration measurement range (P/cm^3)	1 ~ 10^6
Withstand temperature (°C)	up to 250 for aerosol sensor
Sampling flow rate (L/min)	5

Table 3 Measurement parameters and uncertainties [30, 32]

Parameter	Sensor type	Range	Uncertainty
Humidity	Hygrometer	0 ~ 100%	±5%
Water pressure	Strain gage	0 ~ 10 MPa	±0.45 MPa
Vessel pressure	Strain gage	0 ~ 1 MPa	±0.045 MPa
Temperature	Type K thermo-couple	200 ~ 1260 °C	±2.9 °C
Spray flow rate	Ultrasonic	0 ~ 60 L/min	±0.24 L/min

the uncertainties associated with these measurements, all of which fall within acceptable ranges. Temperature and pressure remained stable throughout the experiment. The water pressure and spray flow rate exhibited fluctuations during the initial 20–30 s of spraying but stabilized thereafter. Additionally, the humidity increased progressively and reached saturation a few minutes after the initiation of mist or spray injection [27].

2.7 Experimental procedures

The general procedures for laser-induced aerosol generation and spray scavenging experiments are illustrated in Fig. 6. For different experiments, the 1.5-kW laser irradiated the test specimen inside the UTARTS vessel for 30 s from an optical window. When the laser beam impacted the test specimen, material evaporation occurred, producing a substantial quantity of aerosol particles that were sampled through a line positioned 500 mm above the irradiation zone and 1000 mm below the spray nozzle. To ensure the homogeneity of aerosol dispersion within the vessel, dry compressed air was injected at the bottom of the vessel at a flow rate of 70 L/min for 300 s. This air injection was conducted with the aerosol outlet valve open to prevent the pressurization of the vessel. It is important to note that the interaction between the laser and specimen is expected to generate residual energy during laser irradiation. However, given the size of the UTARTS vessel and the continuous flow of mixed air, this residual energy is unlikely to have any significant effect. By the time the aerosol scavenging process commenced after laser irradiation, the residual energy was expected to dissipate. Furthermore, the temperature and pressure sensors installed inside the UTARTS facility to monitor the experimental conditions recorded no significant variations, confirming the stability of the system during the experiments.

Regarding the subsequent aerosol scavenging processes, generally three conditions, including "spray & no-mist", "spray & neutral mist" and "spray & charged mist", were considered. Mist injection was performed for cases investigating mist effects. For cases using "spray & neutral mist", the neutral-mist injection was performed for 300 s, and idling was kept for another 300 s for aerosol-mist agglomeration.

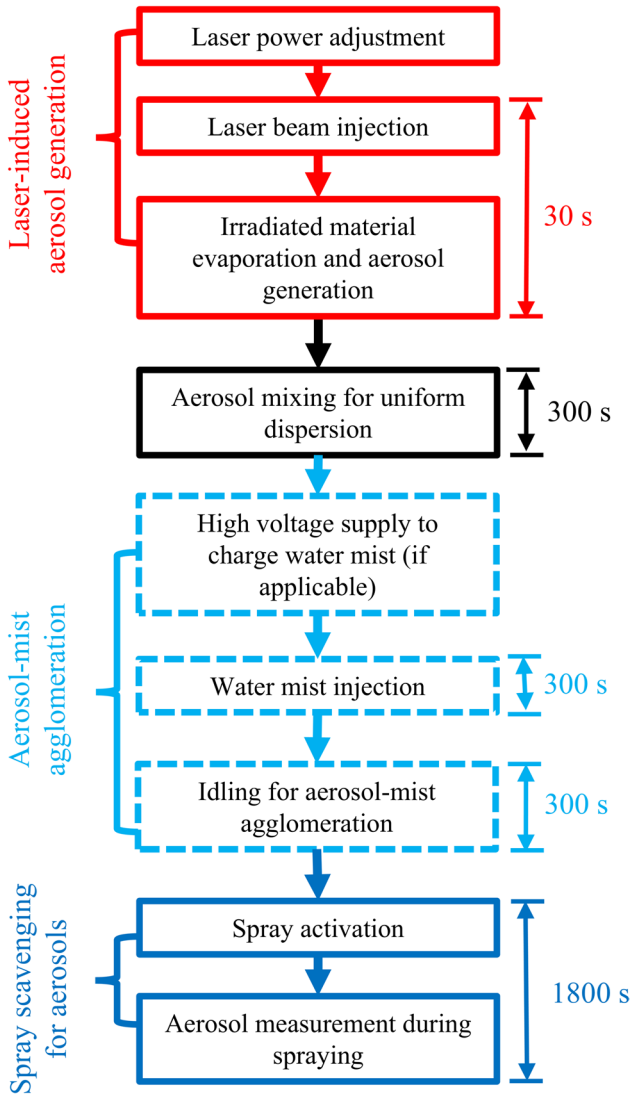

Fig. 6 General procedures for laser-induced aerosol generation and spray scavenging experiments

While for cases using "spray & charged mist", the high-voltage supply was activated to the electrode before the mist injections to ensure mist charging during their injections. A neutral water spray was then injected to remove aerosols. During spray activation, the aerosol particles were sampled and their concentrations were monitored using an aerosol analyzer (Welas 3000). The size distribution data were presented as normalized number concentrations per logarithmic diameter interval.

2.8 Experimental parameters

Table 4 lists the parameters used in the current scavenging experiments for aerosols generated from laser cleaning. Regarding the parameters used for laser-induced aerosol generation, the laser power was fixed at the maximum

Table 4 Parameters in the scavenging experiments for aerosols generated from laser cleaning

Type	Parameter	Value
Aerosol generation	Irradiation power, P_{ir} (kW)	1.5
	Irradiation time, t_{ir} (s)	30
	Irradiation area	Circle ($\Phi = 5$ mm)
	Line distance in each scan (mm)	0.1 for CS&SS; 0.5 for concrete
	Test specimens	CS: 50 mm × 50 mm × 5 mm; SS: 50 mm × 50 mm × 5 mm; Concrete: 150 mm × 150 mm × 30 mm
	Surface coating material	Oxidized layer; CeO_2; ZrO_2
Aerosol scavenging	Spray nozzle	Nozzle 1
	Electrode model	1B for spray charging; 3B for mist charging
	Voltage and polarity for spray charging	− 15 kV
	Voltage and polarity for mist charging	− 10 kV; + 10 kV
	Spray flow rate, Q (L/min)	2; 3; 4
	Mist concentration level	0; High C_{mist}

value (1.5 kW) for the 30-s irradiation to attain an adequate concentration of generated aerosols from varying surface conditions. Similarly, CS, SS, and concrete surfaces coated with CeO_2, ZrO_2, and an oxidized layer (typically for the CS surface) were employed. For the aerosol scavenging parameters, no-mist and high-concentration mist conditions were considered. For mist charging, –10 kV and + 10 kV were both considered to further investigate the effect of polarity on aerosol scavenging in more realistic scenarios.

3 Results and discussion

3.1 Aerosol size distribution and variation during spray

Figure 7 shows the aerosol size distributions and variations during sprays for experiments under different specimen and mist conditions. Focusing on the aerosol concentrations before spraying, it was found that for metal and concrete surfaces, the laser-generated aerosol sizes ranged within the Greenfield gap. It can be seen that the aerosol number concentrations peak at approximately 0.28 μm for metal surfaces and 35 μm for concrete surfaces, caused by the mechanism of aerosol generation with laser interaction. If a laser beam interacts with the material surface, the absorbed energy causes the surface temperature to increase. As the energy density of the laser increased, the temperature eventually reached the vaporization threshold of the material. At this stage, the surface underwent melting and vaporization by laser irradiation, inducing recoil pressure on the molten layer. This recoil pressure (Pr) is intrinsically linked to the saturated vapor pressure, which is determined by the temperature within the molten region [64]. The recoil pressure generated by vaporization intensified with increasing surface temperature. Once this pressure exceeds the surface tension of the molten surface, it drives the vapor–liquid mixture away from the molten pool. Simultaneously, the molten liquid was displaced along the cavity sidewall until expulsion. During laser cleaning, submicron aerosol particles, droplets, and fragments are produced. The formation of fine particles smaller than 1 μm arises from rapid expansion and substantial cooling of the vapor, which is subsequently followed by nucleation and condensation processes [65–67].

Figure 8 shows a schematic of various laser-irradiated surfaces. Notably, our experiments revealed the formation of a substantial number of fine particles. These particles are generated from liquid droplets within the molten layer [65, 66]. For concrete surfaces, a series of chemical and physical reactions occur, primarily driven by the dehydration of calcium hydroxide and decomposition of calcium carbonate, resulting from the release of gases (such as CO_2 and H_2O) from the irradiated zone [12]. With an increase in the energy density, the corresponding temperature rise leads to the melting of the cement and aggregates, forming a thick SiO_2-rich molten pool within the cavity. The pressure generated in this phase propels molten concrete along the sidewalls of the cavity until its ejection. Furthermore, gases released during concrete decomposition encounter the high viscosity of the molten pool, causing them to escape from the surface. Sustained gas production significantly increased the pressure beneath the molten layer, creating a gas bubble within the melt that progressively expanded over time. The difference in the aerosol formation mechanisms for different surfaces leads to different size distributions after their generation.

Regarding the aerosol concentration variation during spraying, as shown in Fig. 7, an obvious reduction in aerosol

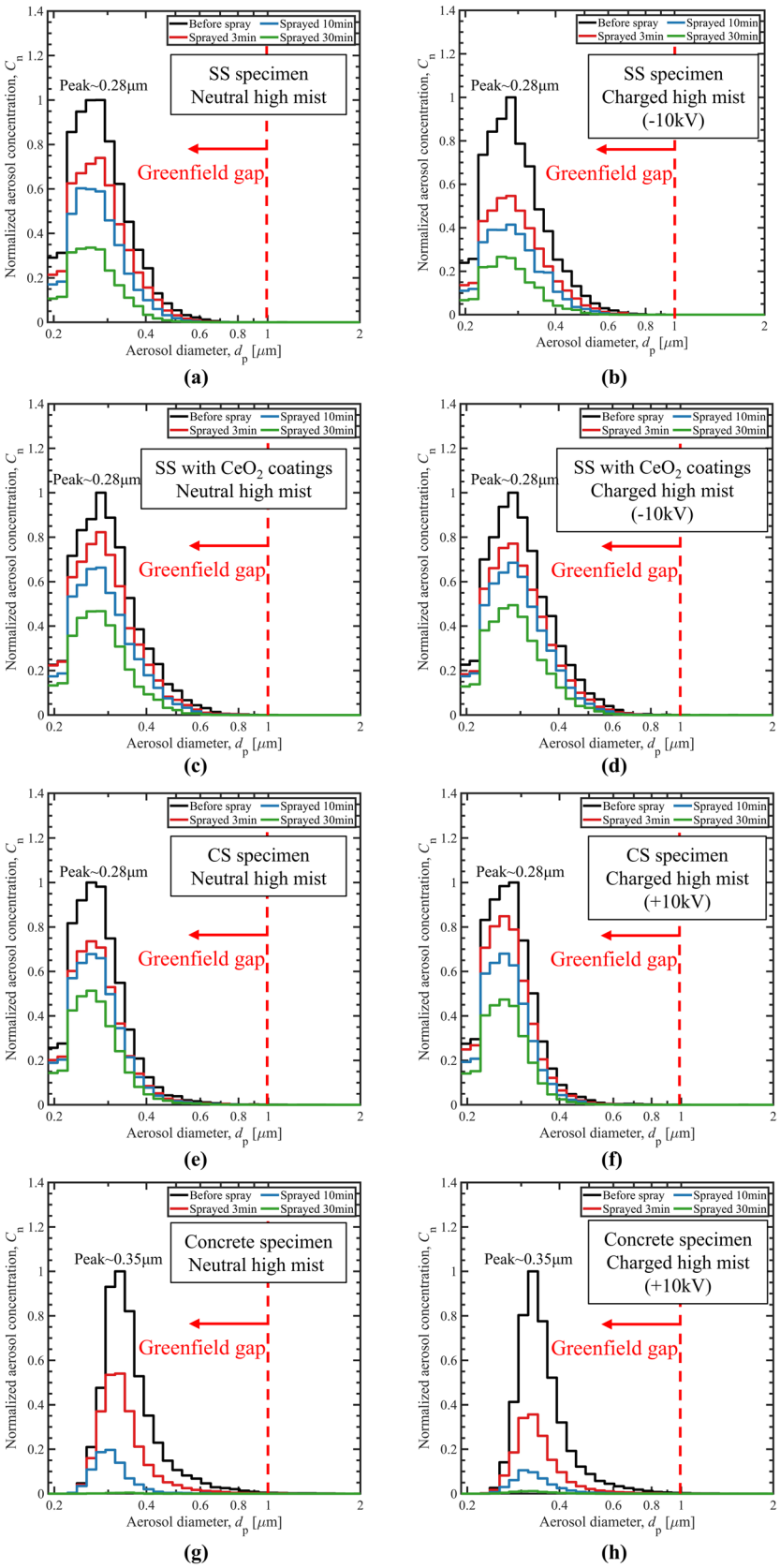

Fig. 7 (Color online) Aerosol size distributions and variations during sprays for experiments under different specimen and mist conditions: **a** SS specimen and neutral high C_{mist}; **b** SS specimen and charged high C_{mist} ($V = -10$ kV); **c** SS specimen with CeO_2 coatings and neutral C_{mist}; **d** SS specimen with CeO_2 coatings and charged high C_{mist} ($V = -10$ kV); **e** CS specimen and neutral high C_{mist}; **f** CS specimen and charged high C_{mist} ($V = +10$ kV); **g** Concrete specimen and neutral high C_{mist}; **h** Concrete specimen and charged high C_{mist} ($V = +10$ kV)

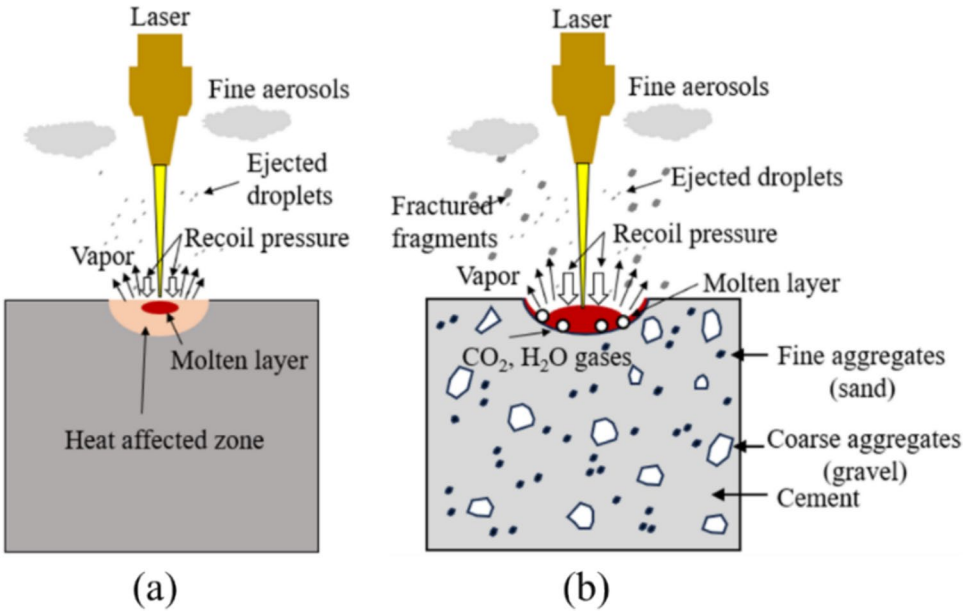

Fig. 8 (Color online) Schematic view of the laser irradiation to specimens for: **a** metal surface, **b** concrete surface [32]

concentration for all sizes can be observed irrespective of experimental conditions. Aerosol particles can be captured by neutral sprayed droplets by mechanical (e.g., Brownian diffusion, inertial impaction, and interception) and phoretic (e.g., diffusio- and thermophoresis) effects. It is noteworthy that, based on our prior experimental measurements [68], the relative humidity within the UTARTS chamber increases from the ambient level (approximately 65%) to 99% following the mist injection or a 6-min spray without mist injection, which is driven by the production of small droplets. Owing to their high velocity relative to the chamber dimensions, the falling time of these droplets was brief. For thermophoresis, the experiments were conducted at room temperature. While localized temperatures at and around the irradiated surface are expected to be very high during laser irradiation (inducing melting, evaporation, and aerosol generation), significant heat removal occurred during the 5-min air mixing phase prior to mist injection. Furthermore, the specimen cooled rapidly once spray activation began. Consequently, the influence of diffusiophoresis and thermophoresis on the capture of aerosol particles near falling spray droplets is expected to be negligible compared to other mechanisms, such as Brownian diffusion, initial impaction, and interception.

By comparing the results of metal and concrete aerosols, it can be found that the spray system can easily remove the concrete, as shown in Fig. 7g and h, where almost all aerosols are removed after 30-min sprays. This can be attributed to the more hydrophilic nature of the concrete aerosol particles (e.g., SiO_2) compared to the SS and CS particles. The concentration peak shifting to smaller sizes is also observable for concrete cases, indicating faster removal of larger-sized aerosols. This variation in aerosol size distribution can be explained by the greater influence of inertial impaction and interception exerted by the spray droplets on larger-sized aerosols. However, for the metal surface cases, as shown in Fig. 7a–f, although faster removal of larger-sized aerosols was found, no apparent peak shifting was found within the 30-min spray due to the low removal efficiency of hydrophobic metal aerosols. Since the aerosol size distribution were found to be concentrated within 0.2 to around 0.6 microns, the aerosol removal efficiencies for 0.2 ~ 0.6 μm are analyzed and discussed in the following sections.

3.2 Quantification for aerosol removal efficiency with different sizes

For the quantitative evaluation of the removal process for aerosol particles of different sizes, the aerosol removal efficiency E is defined as

$$E\left(t_{\text{spray}}\right)\Big|_{d=d_{\text{p}}} = \frac{C_{\text{n}}(0s)\big|_{d=d_{\text{p}}} - C_{\text{n}}\left(t_{\text{spray}}\right)\Big|_{d=d_{\text{p}}}}{C_{\text{n}}(0s)\big|_{d=d_{\text{p}}}}, \tag{1}$$

where t_{spray} is the time since spray activation. From Eq. (1), the global removal efficiency E was determined by the reduction in aerosol number concentration, measured as the decrease from the initial concentration to the value observed at t_{spray}. A higher E value close to 1 indicates more effective and thorough removal of aerosol particles.

In our experiments, it was observed that, during the initial transient spraying phase (e.g., 1–3 min), the aerosol concentration was not spatially consistently distributed when the flow pattern was still developing. Nevertheless, as the spray continued (e.g., 5–30 min) and the flow pattern

stabilized, the discrepancy in the spatial distribution of aerosols was significantly reduced. In addition, preliminary tests conducted at the UTARTS facility indicated that the background loss of aerosol particles (e.g., due to deposition or agglomeration) was negligible when the spray duration exceeded approximately 10 min [68]. Consequently, for the quantitative analyses presented in the following sections, the experimental results obtained at 30 min were considered for the metal surfaces. For the concrete surfaces, as the removal process is comparatively faster and all aerosols are mostly removed after 30-min sprays irrespective of experimental conditions (as shown in Fig. 7g, h), we consider a 10-min removal efficiency for concrete cases.

3.3 Effect of neutral and charged water mist for metal surfaces

Figure 9 shows the removal efficiency under different mist conditions after 30 min sprays for aerosols generated from different metal surfaces irradiated by the laser. As shown in Fig. 9, it can be found that for both metal surfaces, injecting water mist is helpful for improving the aerosol removal efficiency as compared to the aerosol removal efficiency in case without mist injection. This phenomenon can be explained as follows. In the presence of water mist, the diffusiophoresis mechanism compels the aerosol particles within the experimental chamber to migrate toward the water mist surface. Additionally, mist-aerosol coagulation may also occur due to different mechanisms, especially gravitational and Brownian coagulation [27]. Furthermore, the interaction with mist enhances the surface wettability of aerosol particles, thereby increasing the water uptake capability. As a result, the agglomerated aerosol-mist particles exhibit a stronger affinity for spray droplets, accelerating their removal process. The experimental results validated the feasibility of our aerosol-mist agglomeration method for improving the removal of aerosols generated by laser irradiation. This reveals the effectiveness of pre-injection of water mist in improving aerosol scavenging in a more realistic industrial application, such as the Fukushima Daiichi decommissioning.

However, for the SS surface, as shown in Fig. 9a, compared with the neutral-mist case, the aerosol removal efficiency is higher when using a negative charging supply to water mist, and lower when using a positive charging supply. By using the negative charging supply to water mist, the average improvements in SS aerosol removal efficiency were 40% and 3%, respectively, compared to no-mist and neutral-mist cases, respectively. For the CS, as depicted in Fig. 9b, the situation is the opposite. By using the positive charging supply to water mist, the average improvements in the CS aerosol removal efficiency were 44% and 9% compared to the no-mist and neutral-mist cases, respectively. This may be because the crystal structure of the SS surface

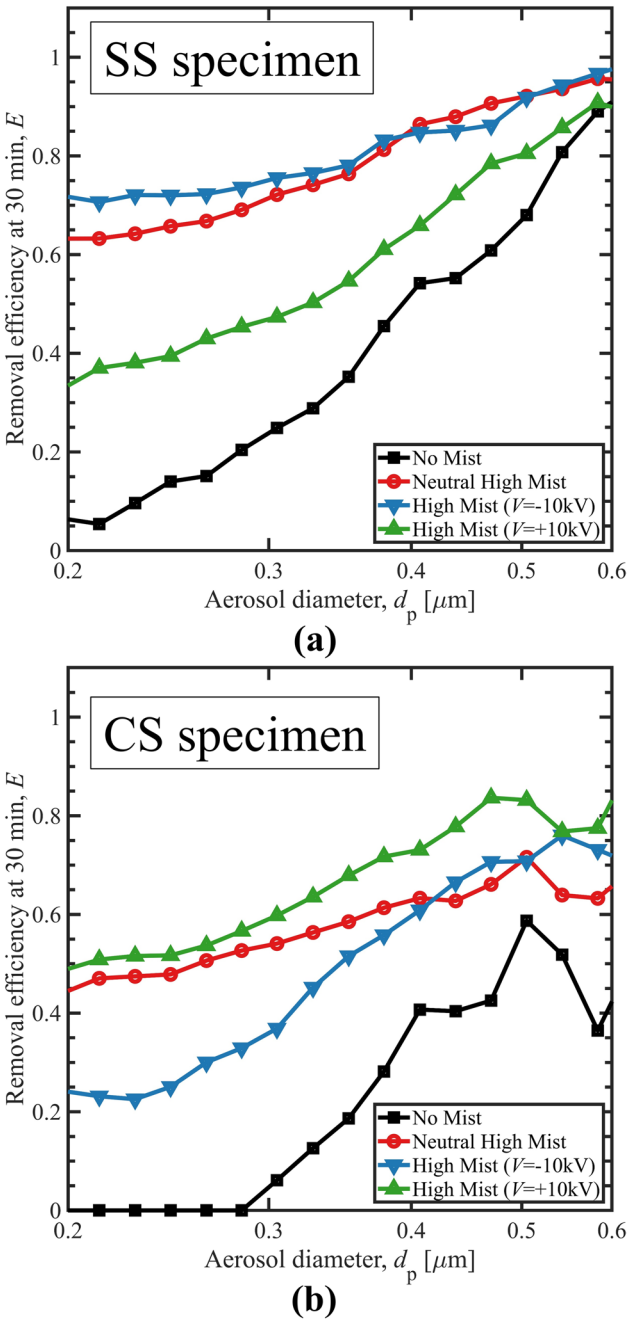

Fig. 9 (Color online) Aerosol removal efficiency under different mist conditions after 30-min sprays for: **a** SS specimens, **b** CS specimens

without coating shows a lower capacity for electron retention and leads to the dominance of negative ion emission during laser irradiation [69, 70], thereby improving the agglomeration between generated aerosols with negative charges and injected water mist with positive charges, which is charged by a negative voltage supply from induction charging. On the other hand, the CS surface is supposed to retain electron emission during laser irradiation, predominantly generating aerosol particles with positive charges. As a result, the

application of a positive voltage supply, which induces negative charges in injected water mist particles, shows a better aerosol scavenging efficiency for the CS surface owing to the enhanced aerosol-mist agglomeration as compared to the neutral-mist case. Conversely, the negative voltage supply to charge the water mist results in a slower removal process for laser-induced aerosol particles from the CS surface.

3.4 Effect of neutral and charged water mist for concrete surfaces

Figure 10 shows the removal efficiency under different mist conditions after 10-min sprays for aerosols generated from concrete surfaces irradiated by a laser. As shown in Fig. 10, it can be found that the pre-injection of water mist is also beneficial for accelerating the aerosol removal process by water spray in comparison with the case without mist injection. Again, this could be attributed to the enlargement of aerosol sizes and improvement in wettability by agglomeration with water mist. The results again indicate the applicability of aerosol-mist agglomeration in facilitating aerosol removal in more realistic engineering scenarios, irrespective of the charging configurations and surface conditions.

However, unlike the metal cases depicted in Fig. 9, as shown in Fig. 10, both negative and positive voltage supplies for charging the water mist seem to improve the scavenging efficiency of concrete aerosol particles as compared to the water mist without charging. For both negatively charged and positively charged cases, the average improvements in the concrete aerosol removal efficiency were 21% and 10%, respectively, compared with the no-mist and neutral-mist cases, respectively. For the concrete case, the differences in aerosol removal efficiency seem to be insignificant for different polarities of voltage supply. This might be because of the large composition of SiO_2 (> 60%) with low electrical conductivity (or even insulation) in concrete, which is different from the conductive metal cases. Therefore, the aerosol particles generated from laser cleaning of concrete surfaces are supposed to be neutral or have a low charging level in predominance compared to those generated from metal surfaces. This leads to an insignificant effect of the charging polarity of the water mist on the scavenging of concrete aerosols. Compared to the case using a neutral mist for the

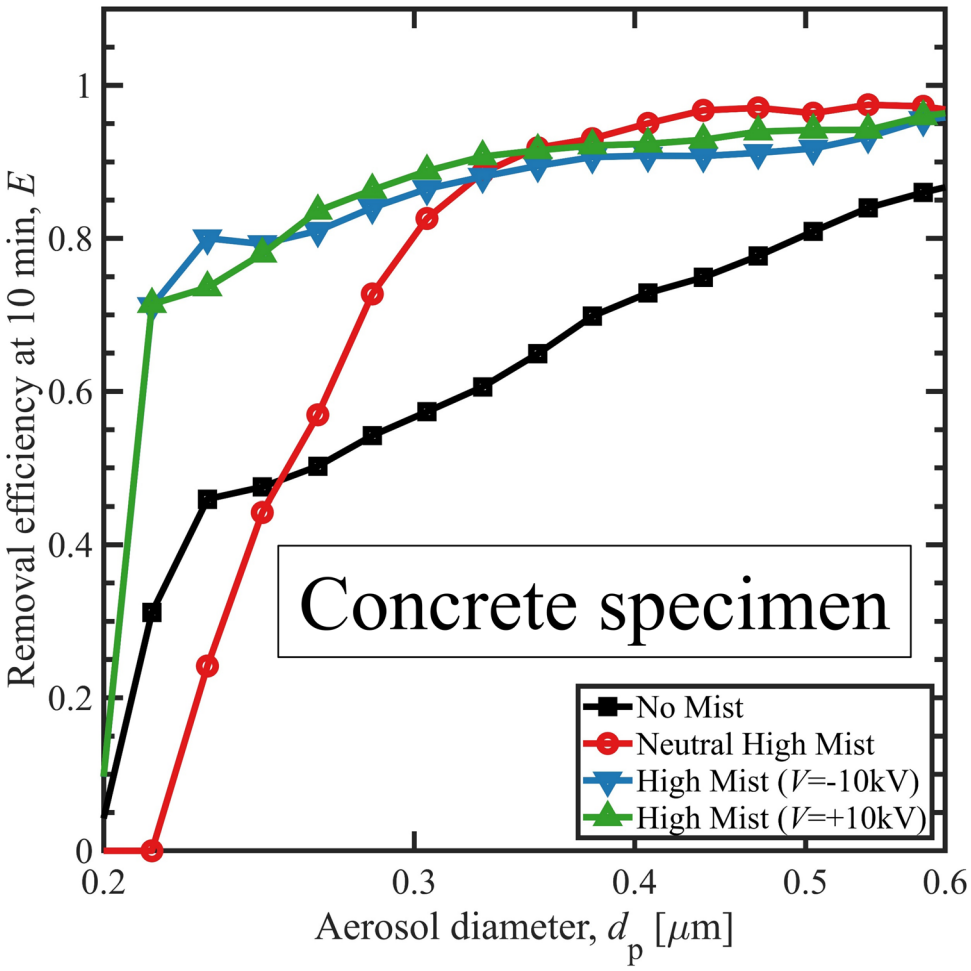

Fig. 10 (Color online) Aerosol removal efficiency under different mist conditions after 10-min sprays for concrete specimens

concrete surface, the improvement shown in the cases using a charged mist was found. One possible reason could be the polarization and induction charging from the charged mist to conductive aerosols generated from the concrete, facilitating the agglomeration of water mist and aerosol particles. The results from the metal concrete surfaces may indicate the different dominant polarities of aerosols generated from distinct materials during laser cleaning operations, which is of great significance for the evaluation of the application of mist/droplet charging techniques to the Fukushima Daiichi decommissioning and other environmental chemical applications.

3.5 Effect of neutral and charged mist for metal surfaces with different coatings

A comparison of the performances of neutral and charged mist in the scavenging of aerosols generated from different surfaces with coatings is shown in Fig. 11. Our experimental results suggest predominant charge states for aerosols generated from metal specimens under different surface conditions. Table 5 summarizes the estimated polarities of aerosol charges under different surface conditions. By comparing the cases using neutral mist and mist charged by negative voltage shown in Figs. 9a and 11a, it can be observed that although the applied negative voltage is helpful for the improved scavenging of aerosols generated from the pure SS surface, the CeO_2 coating on the SS surface seems to reduce this beneficial effect triggered by the pre-injection of mist charged by negative voltage, or may even result in worse performance. For the cases using ZrO_2 coatings, it is clear that the ZrO_2 coating on SS leads to the ineffective application of mist charged by a negative voltage. Similar opposite-ness between the uncoated and CeO_2 coated surfaces can also be found for the CS cases by comparing Figs. 9b and 11b. This may reveal the influence of surface coating on the predominant polarity of aerosols generated during laser cleaning. When an aerosol particle collides with a charged water mist particle, three forces generally act on the aerosol particle: water surface tension, particle inertial force, and electrical attractive force between the aerosol and mist. The Coulomb attractive force accelerates the particle toward the mist, and the electrical attractive force continues to act on the particle until it comes into mechanical contact with the mist surface. After mechanical contact, the Coulomb force still acts for a short time owing to charge relaxation. This electrical force counteracts the rebounding force of the water surface tension, leading to a gentle landing and capture of particles on the droplet surface. This mechanism decreases the probability of particle re-entrainment by rebounding compared to when the particle and droplet are neutral and provides a higher capture efficiency for opposite-charged mist droplets [71].

Because the negative voltage power supply to the electrode would lead to the sprayed droplets being charged positively by induction charging, the results shown in Fig. 11a and b may indicate that the ZrO_2 and CeO_2 coatings on the SS surfaces are expected to cause less generation of negatively charged aerosols during laser cleaning. In contrast, as shown in Fig. 11c, the surface coatings seem to result in more generation of negatively charged aerosols on the CS surfaces. These different influences of the surface coating on the dominant polarity of aerosols generated from different substrate materials may result from the different crystal structures of the materials. During laser irradiation, the efficiency and predominance of electron emission processes, such as thermionic emission (electron emission induced by high temperatures), photoelectric effect (electron emission due to photon interaction), and field emission (electron emission influenced by strong electric fields), can be affected by the crystallographic orientation of the metal surface owing to variations in the electronic properties and atomic arrangement [72–77]. In addition, as the metal surface is heated and potentially melted or vaporized by a laser, the ejected material can form particles via condensation and solidification. The charge state of these particles depends on the nature of the charge carriers involved in their formation. The coatings on the SS surface probably enhance the predominance of positive ion emission due to more effective electron retention, resulting in the generation of more positively charged particles, whereas CS may have the opposite effect.

3.6 Effect of metal surface condition

Figure 12 displays the effect of surface conditions on the scavenging of aerosols generated from different surfaces with mist charging. The injected water mist was electrically charged by a –10 kV voltage supply, which means that the water mist carried positive charges. As shown in Fig. 12a, for the SS substrate, the surface coating seems to restrain aerosol scavenging when using mist with positive charges. This may indicate that the CeO_2 and ZrO_2 coatings on the SS surfaces can probably reduce the generation of negatively charged aerosols during laser cleaning owing to the change in surface conditions. However, as displayed in Fig. 12b, the surface coatings on the CS surfaces seem to intensify the generation of negatively charged aerosols. Corresponding to the findings in the previous sections, this may have resulted from the different crystal structures of the materials and electron emission characteristics during laser irradiation. These results may again reveal the influence of the surface coating on diminishing or even changing the predominant polarity of aerosols generated during laser cleaning, although further detailed investigation and exploration are still required. The current findings on the influence

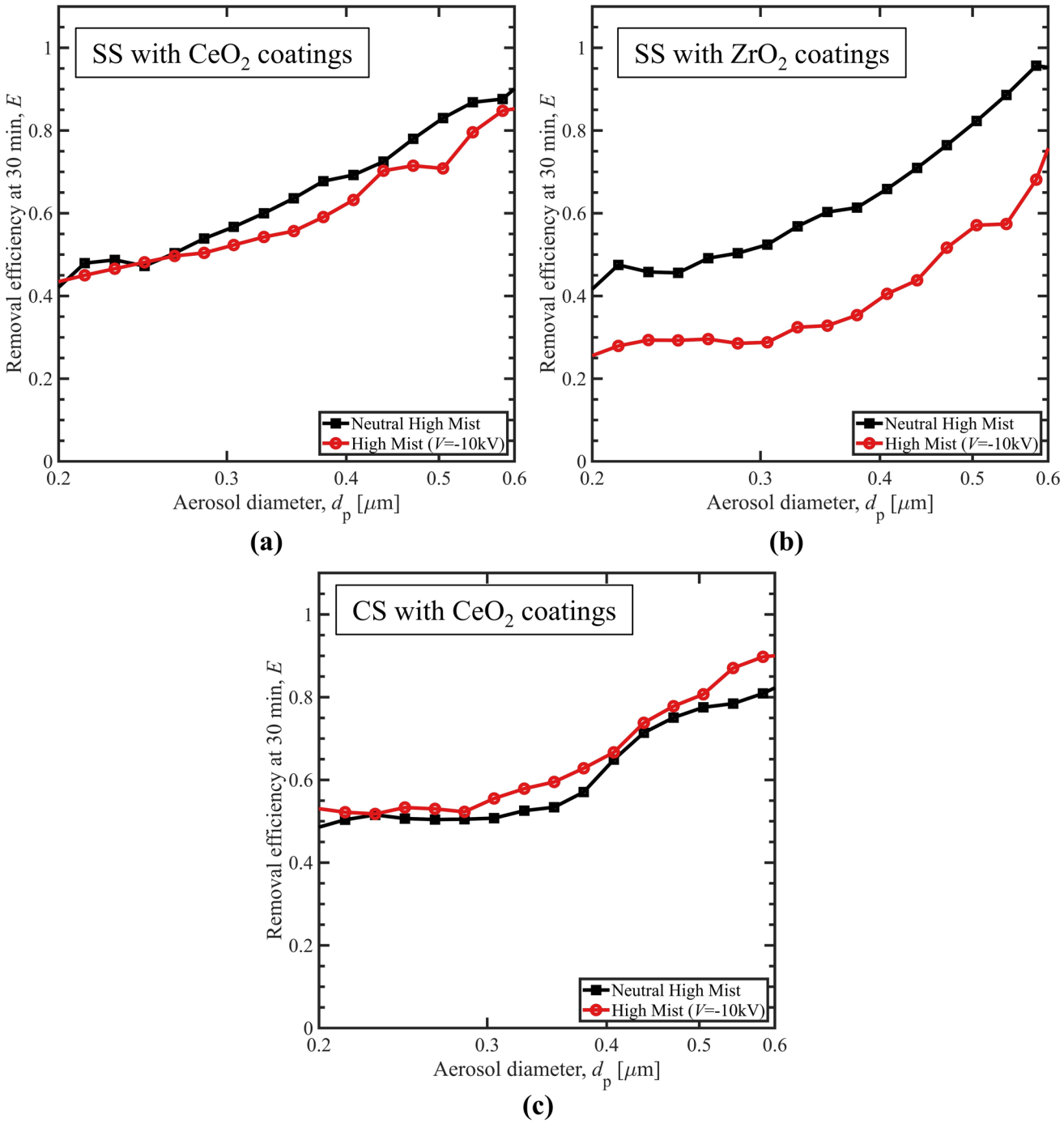

Fig. 11 Comparison of the performance of neutral mist and charged mist in the scavenging of aerosols generated from different surfaces with coatings: **a** SS-CeO_2, **b** SS-ZrO_2, **c** CS-CeO_2

of surface conditions on the charging characteristics of generated aerosols could provide critical insights for developing technical strategies for the dismantling and decommissioning processes of the Fukushima Daiichi nuclear power plant.

4 Conclusion

The efficient removal of harmful aerosols plays a crucial role in gas purification processes aimed at mitigating

Table 5 Estimated polarity of the charge of laser-generated aerosols from metal specimens under different surface conditions

Specimen material	Coating condition	Estimated aerosol charge
SS	Uncoated	Predominantly negative charge
	CeO_2 coating	Reduced negative charge or predominantly positive charge
	ZrO_2 coating	Predominantly positive charges
CS	Uncoated	Predominantly positive charges
	CeO_2 coating	Predominantly negative charges
	Oxidized layer	Predominantly negative charges

environmental pollution across various chemical industrial applications, including the decommissioning of nuclear reactors. In particular, during the dismantling of the Fukushima Daiichi nuclear reactors, it is essential to control greenfield-gap radioactive aerosol particles to prevent the release of radioactivity into the environment and to minimize radiation exposure risks for both workers and the public. Techniques for improving the aerosol removal efficiency must be validated in realistic scenarios.

In the present study, an experimental investigation on the removal of aerosols generated from laser cleaning using spray with pre-injection of neutral/charged water mist was performed in our UTARTS facility to validate the applicability of the aerosol-mist agglomeration technique and attain more knowledge on laser-induced aerosol generation and spray scavenging under more realistic conditions in view of the Fukushima Daiichi decommissioning. The experimental results validated the feasibility and applicability of the pre-injection of water mist for accelerating the scavenging processes of aerosols generated by laser irradiation. Proper mist charging was also beneficial for facilitating aerosol scavenging. The average improvements were 40%, 44%, and 21% for SS, CS, and concrete, respectively. Furthermore, different polarities of the charged mist showed opposite influences on the aerosol removal efficiency for different irradiated materials, indicating that the dominant polarity of aerosols generated may be different for different materials during laser irradiation, which is attributed to the different crystal structures of the materials and electron emission characteristics during laser irradiation. Based on experiments using a negative charging voltage, the surface coating was found to be effective for affecting (or even changing) the dominant polarity of aerosols generated during laser cleaning. An investigation of the effects of positive charging on coated surfaces will be conducted in the future to further elucidate these polarity-dependent mechanisms. The current study provides important knowledge on the improvement of aerosol removal and gas purification in the Fukushima Daiichi decommissioning and various environmental chemical

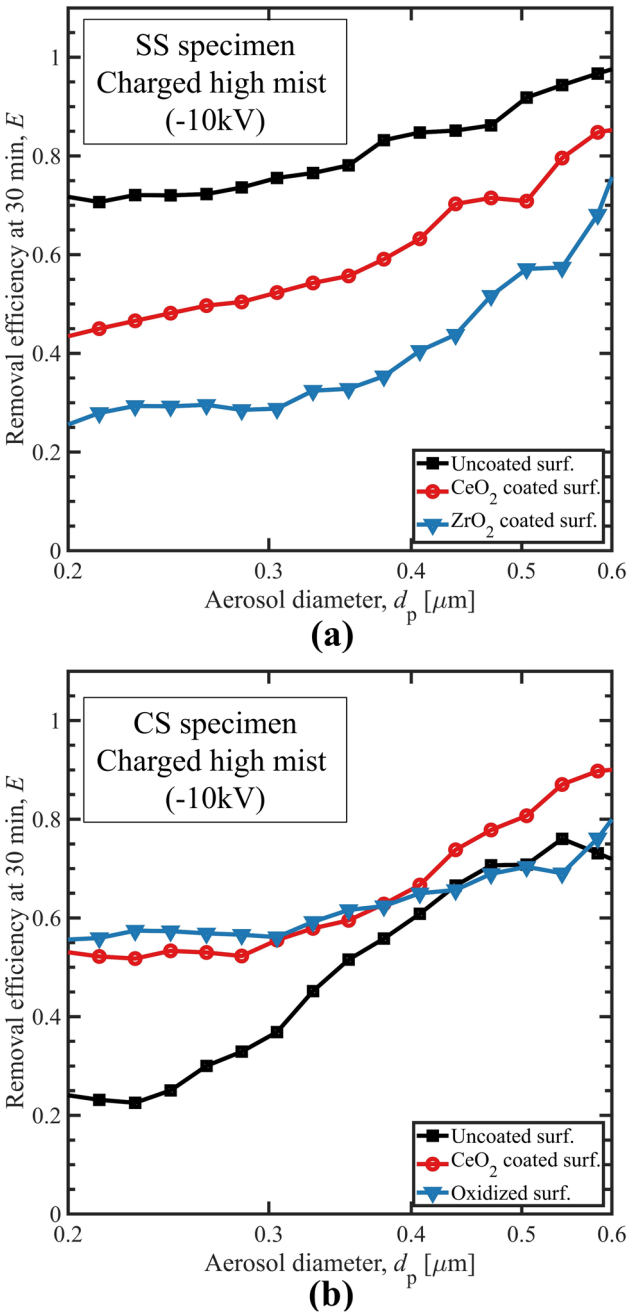

Fig. 12 Effect of surface condition in the scavenging of aerosols generated from different surfaces with mist charging for: **a** SS specimens, **b** CS specimens

engineering processes. Future studies should focus on the detailed characterization of aerosols generated from laser irradiation (e.g., dominant polarity), including laser cleaning and cutting. The understanding and data from this investigation are expected to be used for formulating technical strategies for Fukushima Daiichi decommissioning and developing relevant models of laser-induced aerosol generation and aerosol spray scavenging for wide

applications in environmental and chemical engineering, such as gas decontamination, air purification, and pollution control.

Author contributions All authors contributed to the study conception and design. Material preparation, data collection and analysis were performed by Ruicong Xu, Avadhesh Kumar Sharma, Zeeshan Ahmed, Ravinder Kumar, Laffolley Hugo, Shuichiro Miwa and Atsushi Kosuge. The first draft of the manuscript was written by Ruicong Xu, and all authors commented on previous versions of the manuscript. All authors read and approved the final manuscript.

Funding Open Access funding provided by The University of Tokyo.

Data availability The data that support the findings of this study are available in Science Data Bank at https://cstr.cn/31253.11.sciencedb.26339 and https://doi.org/10.57760/sciencedb.26339.

Declarations

Conflict of interest The authors declare that they have no competing interests.

References

1. N. Wang, P. Zheng, R. Wang et al., Homogeneous and heterogeneous atmospheric ozonolysis of acrylonitrile on the mineral dust aerosols surface. J. Environ. Chem. Eng. **9**(6), 106654 (2021). https://doi.org/10.1016/j.jece.2021.106654
2. S. Salana, V. Verma, Review of in vitro studies evaluating respiratory toxicity of aerosols: impact of cell types, chemical composition, and atmospheric processing. Environ Sci Process Impacts **26**(11), 1922–1954 (2024). https://doi.org/10.1039/D4EM00475B
3. E. Porcheron, C. Dazon, T. Gelain et al., Fukushima Daiichi fuel debris retrieval: results of aerosol characterization during laser cutting of non-radioactive corium simulants. J. Nucl. Sci. Technol. **58**(1), 87–99 (2021). https://doi.org/10.1080/00223131.2020.1806135
4. E. Ozdemir, S. Miwa, E. Porcheron et al., Aerosol deposition and dispersion during nuclear reactor decommissioning. Nucl. Eng. Des. **414**, 112623 (2023). https://doi.org/10.1016/j.nucengdes.2023.112623
5. E. Porcheron, Y. Leblois, T. Gelain et al., Aerosol mitigation means for Fukushima Daiichi fuel debris removal, ASME 2023 International Conference on Environmental Remediation and Radioactive Waste Management, Stuttgart, Germany, 2023.
6. J. Onodera, H. Yabuta, T. Nishizoro et al., Characterization of aerosols from dismantling work of experimental nuclear power reactor decommissioning. J. Aerosol Sci. **22**, S747–S750 (1991). https://doi.org/10.1016/S0021-8502(05)80208-3
7. R. Kumar, Z. Ahmed, R. Xu et al., Investigation of aerosol particle dispersion and removal via non-reacting gas for Fukushima Daiichi plant decommissioning. J. Environ. Chem. Eng. **13**(4), 117246 (2025). https://doi.org/10.1016/j.jece.2025.117246
8. Inter-Ministerial Council for Contaminated Water and Decommissioning Issues, Mid-and-Long-Term roadmap towards the decommissioning of TEPCO's Fukushima Daiichi nuclear power station, 2019. https://www.meti.go.jp/english/earthquake/nuclear/decommissioning/pdf/20191227_3.pdf
9. A.B. Lopez, E. Assunção, L. Quintino et al., High-power fiber laser cutting parameter optimization for nuclear decommissioning. Nucl. Eng. Technol. **49**(4), 865–872 (2017). https://doi.org/10.1016/j.net.2017.02.004
10. K. Tamura, Si. Toyama, Laser cutting performances for thick steel specimens studied by molten metal removal conditions. J. Nucl. Sci. Technol. **54**(9), 1011–1017 (2017). https://doi.org/10.1080/00223131.2017.1344156
11. A.K. Sharma, H. Liang, R. Xu et al., Radioactive aerosol control and decontamination in the decommissioning of the Fukushima Daiichi Nuclear Power Station. Nucl. Technol. **209**(12), 2030–2043 (2023). https://doi.org/10.1080/00295450.2023.2186675
12. N.P. Long, H. Daido, T. Yamada et al., Experimental characterization of concrete removal by high-power quasicontinuous wave fiber laser irradiation. J. Laser Appl. **29**(4), 041501 (2017). https://doi.org/10.2351/1.5008326
13. E. Porcheron, Y. Leblois, T. Gelain et al., Assessment of spray and pool scrubbing efficiencies for means of mitigation against aerosol dispersion in the context of fuel debris retrieval at Fukushima Daiichi: Part I. J. Nucl. Eng. Radiat. Sci. **8**(3), 031701 (2022). https://doi.org/10.1115/1.4051611
14. E. Porcheron, Y. Leblois, T. Gelain et al., Assessment of spray and pool scrubbing efficiencies for means of mitigation against aerosol dispersion in the context of fuel debris retrieval at Fukushima Daiichi: Part II. J. Nucl. Eng. Radiat. Sci. **8**(3), 031702 (2022). https://doi.org/10.1115/1.4051538
15. C. Dazon, E. Porcheron, C. Journeau et al., Characterization of chemical composition and particle size distribution of aerosols released during laser cutting of fuel debris simulants. J. Environ. Chem. Eng. **8**(4), 103872 (2020). https://doi.org/10.1016/j.jece.2020.103872
16. C. Journeau, D. Roulet, E. Porcheron et al., Fukushima Daiichi fuel debris simulant materials for the development of cutting and collection technologies. J. Nucl. Sci. Technol. **55**(9), 985–995 (2018). https://doi.org/10.1080/00223131.2018.1462267
17. E. Porcheron, S. Peillon, T. Gelain et al., Analysis of aerosol emission and dispersion during the laser cutting of Fukushima fuel debris simulants, 26th International Conference on Nuclear Engineering (ICONE26), London, UK, 2018.
18. E. Porcheron, P. Lemaitre, D. Marchand et al., Experimental and numerical approaches of aerosol removal in spray conditions for containment application. Nucl. Eng. Des. **240**(2), 336–343 (2010). https://doi.org/10.1016/j.nucengdes.2008.08.023
19. S. Gupta, E. Schmidt, M.L. Freitag et al., Experimental investigations on containment spray performance under severe accident conditions. The 8th European Review Meeting on Severe Accident Research (ERMSAR), Warsaw, Poland, 2017.
20. A.K. Dwivedi, A. Khan, S.N. Tripathi et al., Aerosol depositional characteristics in piping assembly under varying flow conditions. Prog. Nucl. Energy **116**, 148–157 (2019). https://doi.org/10.1016/j.pnucene.2019.04.007
21. J. Yang, D.Y. Lee, S. Miwa et al., Overview of filtered containment venting system in nuclear power plants in Asia. Ann. Nucl. Energy **119**, 87–97 (2018). https://doi.org/10.1016/j.anucene.2018.03.047

22. E. Ozdemir, R. Xu, S. Miwa et al., Numerical and experimental approach for dust dispersion and deposition behavior for safe decommissioning activities. Energy Sources Part A Recover. Util. Environ. Eff. **46**(1), 8070–8087 (2024). https://doi.org/10.1080/15567036.2024.2368494
23. E. Porcheron, P. Lemaitre, A. Nuboer et al., Experimental investigation in the TOSQAN facility of heat and mass transfers in a spray for containment application. Nucl. Eng. Des. **237**(15–17), 1862–1871 (2007). https://doi.org/10.1016/j.nucengdes.2007.01.018
24. A. del Corno, S. Morandi, F. Parozzi et al., Experiments on aerosol removal by high-pressure water spray. Nucl. Eng. Des. **311**, 28–34 (2017). https://doi.org/10.1016/j.nucengdes.2016.06.043
25. H. Yu, H. Gu, Z. Sun et al., Study on the influence of droplet agglomeration on the removal of aerosol by spray system. Prog. Nucl. Energy **140**, 103903 (2021). https://doi.org/10.1016/j.pnucene.2021.103903
26. C. Kaltenbach, E. Laurien, CFD simulation of aerosol particle removal by water spray in the model containment THAI. J. Aerosol Sci. **120**, 62–81 (2018). https://doi.org/10.1016/j.jaerosci.2018.03.005
27. H. Liang, Q. Zhou, N. Erkan et al., Improvement of aerosol spray scavenging efficiency with water mist. J. Aerosol Sci. **153**, 105697 (2021). https://doi.org/10.1016/j.jaerosci.2020.105697
28. H. Liang, Q. Zhou, N. Erkan et al., Effect of spray properties on aerosol scavenging efficiency with water mist. Aerosol Sci. Technol. **56**(1), 29–45 (2022). https://doi.org/10.1080/02786826.2021.1966377
29. B. Blaisot, M. Pellegrini, H. Liang et al., Study of the aerosol dispersion control by a spray system during Fukushima Daiichi fuel debris retrieval. 19th International Topical Meeting on Nuclear Reactor Thermal Hydraulics (NURETH-19), Brussels, Belgium, 2022.
30. A.K. Sharma, R. Xu, Z. Ahmed et al., Scavenging of laser-generated aerosols with electrostatic-charged spray droplets. J. Aerosol Sci. **174**, 106254 (2023). https://doi.org/10.1016/j.jaerosci.2023.106254
31. R. Xu, A.K. Sharma, E. Ozdemir et al., Experimental investigation on effective aerosol scavenging using different spray configurations with pre-injection of water mist for Fukushima Daiichi decommissioning. Nucl. Sci. Tech. **35**, 42 (2024). https://doi.org/10.1007/s41365-024-01401-9
32. A.K. Sharma, R. Xu, Z. Ahmed et al., Investigation of aerosol generation through laser cleaning of various surfaces and optimization of mist & spray scavenging. J. Aerosol Sci. **177**, 106329 (2024). https://doi.org/10.1016/j.jaerosci.2023.106329
33. H. Liang, N. Erkan, Q. Zhou et al., Effect of vessel size scale on the aerosol spray scavenging efficiency with water mist. J. Aerosol Sci. **159**, 105853 (2022). https://doi.org/10.1016/j.jaerosci.2021.105853
34. R. Xu, A.K. Sharma, E. Ozdemir et al., Numerical investigation on improved spray system for efficient aerosol removal during the decommissioning of Fukushima Daiichi nuclear power plants. Nucl. Eng. Des. **419**, 112960 (2024). https://doi.org/10.1016/j.nucengdes.2024.112960
35. F. Di Natale, C. Carotenuto, L. D'Addio et al., Effect of gas temperature on the capture of charged particles by oppositely charged water droplets. Aerosol Sci. Technol. **50**(2), 110–117 (2016). https://doi.org/10.1080/02786826.2015.1131810
36. Z. Ahmed, R. Kumar, A.K. Sharma et al., Effect of wettability and particle size on aerosol removal efficiency in charged and neutral water spray systems. J. Environ. Chem. Eng. **13**(2), 115822 (2025). https://doi.org/10.1016/j.jece.2025.115822
37. K. Ardon-Dryer, Y.W. Huang, D.J. Cziczo, Laboratory studies of collection efficiency of sub-micrometer aerosol particles by cloud droplets on a single-droplet basis. Atmos. Chem. Phys. **15**(16), 9159–9171 (2015). https://doi.org/10.5194/acp-15-9159-2015
38. S.M. Greenfield, Rain scavenging of radioactive particulate matter from the atmosphere. J. Atmos. Sci. **14**(2), 115–125 (1957). https://doi.org/10.1175/1520-0469(1957)014%3c0115:RSORPM%3e2.0.CO;2
39. Q. Zhou, T. Saito, S. Suzuki et al., Microparticles with diverse sizes and morphologies from mechanical and laser cutting of fuel debris simulants and geopolymer as a covering material. J. Nucl. Sci. Technol. **58**(4), 461–472 (2021). https://doi.org/10.1080/00223131.2020.1869623
40. A. Jaworek, A. Krupa, A.T. Sobczyk et al., Submicron particles removal by charged sprays. Fundam. J. Electrostat. **71**(3), 345–350 (2013). https://doi.org/10.1016/j.elstat.2012.11.028
41. K. Amaya, A. Bayat, Determining effects of induction electrode geometry on charging efficiency of droplets in pesticide electrostatic spraying applications. Smart Agric. Technol. **4**, 100190 (2023). https://doi.org/10.1016/j.atech.2023.100190
42. A. Brentjes, B. Jansen, A.K. Pozarlik, Spray characteristics of an air-assisted electrostatic atomiser. J. Electrostat. **115**, 103654 (2022). https://doi.org/10.1016/j.elstat.2021.103654
43. S. Dai, J. Zhang, W. Jia et al., Experimental study on the droplet size and charge-to-mass ratio of an air-assisted electrostatic nozzle. Agriculture **12**(6), 889 (2022). https://doi.org/10.3390/agriculture12060889
44. M.K. Patel, C. Ghanshyam, P. Kapur, Characterization of electrode material for electrostatic spray charging: theoretical and engineering practices. J. Electrostat. **71**(1), 55–60 (2013). https://doi.org/10.1016/j.elstat.2012.11.019
45. A. Marchewicz, A.T. Sobczyk, A. Krupa et al., Induction charging of water spray produced by pressure atomizer. Int. J. Heat Mass Transf. **135**, 631–648 (2019). https://doi.org/10.1016/j.ijheatmasstransfer.2019.02.013
46. S. Zhao, G.S.P. Castle, K. Adamiak, Comparison of conduction and induction charging in liquid spraying. J. Electrostat. **63**(6), 871–876 (2005). https://doi.org/10.1016/j.elstat.2005.03.048
47. L. D'Addio, Wet electrostatic scrubbing for high efficiency submicron particle capture, Ingegneria chimica, Università degli Studi di Napoli Federico II, Napoli, Italy, 2011.
48. R. Xu, A.K. Sharma, S. Miwa et al., Development of improved spray system with effective electrical electrodes for aerosol removal: an experimental study in UTARTS facility. J. Aerosol Sci. **181**, 106431 (2024). https://doi.org/10.1016/j.jaerosci.2024.106431
49. J. Gao, J. Liu, J. Gao et al., Modelling and experimental study on agglomeration of particles from coal combustion in multistage spouted fluidized tower. Adv. Powder Technol. **20**(4), 375–382 (2009). https://doi.org/10.1016/j.apt.2009.06.005
50. J. Yan, L. Chen, L. Yang, Combined effect of acoustic agglomeration and vapor condensation on fine particles removal. Chem. Eng. J. **290**, 319–327 (2016). https://doi.org/10.1016/j.cej.2016.01.075
51. T.L. Hoffmann, Environmental implications of acoustic aerosol agglomeration. Ultrasonics **38**(1), 353–357 (2000). https://doi.org/10.1016/S0041-624X(99)00184-5
52. T. Watanabe, F. Tochikubo, Y. Koizurni et al., Submicron particle agglomeration by an electrostatic agglomerator. J. Electrostat. **34**(4), 367–383 (1995). https://doi.org/10.1016/0304-3886(95)93833-5
53. A. Dépée, P. Lemaitre, T. Gelain et al., Theoretical study of aerosol particle electroscavenging by clouds. J. Aerosol Sci. **135**, 1–20 (2019). https://doi.org/10.1016/j.jaerosci.2019.04.001
54. H.R. Pruppacher, J.D. Klett, Microphysics of clouds and precipitation (Atmospheric and Oceanographic Sciences Library, 18), Springer, 1996.

55. L.-P. Wang, A.S. Wexler, Y. Zhou, Statistical mechanical descriptions of turbulent coagulation. Phys. Fluids **10**(10), 2647–2651 (1998). https://doi.org/10.1063/1.869777
56. S.K. Friedlander, *Smoke, dust, and haze* (Oxford University Press, New York, 2000)
57. H. Yang, C.J. Hogan, Collision rate coefficient for charged dust grains in the presence of linear shear. Phys. Rev. E **96**(3), 032911 (2017). https://doi.org/10.1103/PhysRevE.96.032911
58. R. Xu, A.K. Sharma, E. Ozdemir et al., Investigation on aerosol spray scavenging by using a multi-hole nozzle with water mist for decommissioning of Fukushima Daiichi power plants, 30th International Conference on Nuclear Engineering (ICONE30), Kyoto, Japan, 2023. https://doi.org/10.1299/jsmeicone.2023.30.1304
59. R. Xu, A.K. Sharma, S. Miwa et al., Improvement of aerosol spray scavenging efficiency by pre-injecting electrically charged water mist. J. Environ. Chem. Eng. **12**(6), 114608 (2024). https://doi.org/10.1016/j.jece.2024.114608
60. R. Xu, A.K. Sharma, R. Kumar et al., Efficient radioactive aerosol removal with the development of water mist pre-injection methods and advanced spray charging system for safe Fukushima Daiichi decommissioning: insights from recent experimental studies in UTARTS facility. J. Nucl. Sci. Technol. (2025). https://doi.org/10.1080/00223131.2025.2495076
61. G. Pyrgiotakis, P. Vedantam, C. Cirenza et al., Optimization of a nanotechnology based antimicrobial platform for food safety applications using engineered water nanostructures (EWNS). Sci. Rep. **6**(1), 21073 (2016). https://doi.org/10.1038/srep21073
62. J. Tang, H. Wang, A. Gomez, Controlled nanoparticle synthesis via opposite-polarity electrospray pyrolysis. J. Aerosol Sci. **113**, 201–211 (2017). https://doi.org/10.1016/j.jaerosci.2017.07.001
63. A. Pelesz, T. Czapka, Empirical and numerical analysis of conduction and induction charging of droplets in a three-electrode system. Energies **13**(2), 469 (2020). https://doi.org/10.3390/en13020469
64. V. Semak, A. Matsunawa, The role of recoil pressure in energy balance during laser materials processing. J. Phys. D Appl. Phys. **30**(18), 2541–2552 (1997). https://doi.org/10.1088/0022-3727/30/18/008
65. R. Hergenröder, Laser-generated aerosols in laser ablation for inductively coupled plasma spectrometry. Spectrochim. Acta B At. Spectrosc. **61**(3), 284–300 (2006). https://doi.org/10.1016/j.sab.2006.02.001
66. C. Liu, X. Mao, S.S. Mao et al., Particle size dependent chemistry from laser ablation of brass. Anal. Chem. **77**(20), 6687–6691 (2005). https://doi.org/10.1021/ac0508696
67. Y. He, H. Xie, Y. Ge et al., Laser cutting technologies and corresponding pollution control strategy. Processes **10**(4), 732 (2022). https://doi.org/10.3390/pr10040732
68. H. Liang, Development of an effective spray system for aerosol dispersion control during the decommissioning of Fukushima Daiichi Nuclear Power Plant. Department of Nuclear Engineering and Management, The University of Tokyo, Tokyo, Japan, 2020.
69. V. Augugliaro, V. Loddo, M. Pagliaro et al., Clean by light irradiation: Practical applications of supported TiO_2. Royal Society of Chemistry, 2010.
70. M. Domaschke, Aerosol synthesis and characterization of ultrafine nanoparticles, domaschke, maximilian, Friedrich-Alexander-Universität Erlangen-Nürnberg, München, Germany.
71. S. Sumiyoshitani, T. Okada, M. Hara et al., Direct observation of the collection process for dust particles from an air stream by a charged water droplet. IEEE Trans. Ind. Appl. **IA-20**(2), 274–281 (1984). https://doi.org/10.1109/TIA.1984.4504408
72. H.-F. Cheng, Y.-S. Hsieh, Y.-C. Chen et al., Laser irradiation effect on electron field emission properties of carbon nanotubes. Diamond Relat. Mater. **13**(4), 1004–1007 (2004). https://doi.org/10.1016/j.diamond.2004.01.043
73. C. Herring, M.H. Nichols, Thermionic emission. Rev. Mod. Phys. **21**(2), 185–270 (1949). https://doi.org/10.1103/RevModPhys.21.185
74. E.M. Logothetis, P.L. Hartman, Laser-induced electron emission from solids: many-photon photoelectric effects and thermionic emission. Phys. Rev. **187**(2), 460–474 (1969). https://doi.org/10.1103/PhysRev.187.460
75. H. Palneedi, J.H. Park, D. Maurya et al., Laser irradiation of metal oxide films and nanostructures: applications and advances. Adv. Mater. **30**(14), 1705148 (2018). https://doi.org/10.1002/adma.201705148
76. A.A. Sorokin, S.V. Bobashev, T. Feigl et al., Photoelectric effect at ultrahigh intensities. Phys. Rev. Lett. **99**(21), 213002 (2007). https://doi.org/10.1103/PhysRevLett.99.213002
77. T. Wang, J. Guo, J. Shao et al., Ultrafast thermionic emission from metal irradiated using a femtosecond laser and an electric field in combination. Phys. Plasmas **22**(3), 033106 (2015). https://doi.org/10.1063/1.4914164

Authors and Affiliations

Ruicong Xu[1,2] · Avadhesh Kumar Sharma[3] · Zeeshan Ahmed[1] · Ravinder Kumar[1] · Laffolley Hugo[4] · Ryo Yokoyama[1,2] · Shuichiro Miwa[1,2] · Shunichi Suzuki[5] · Atsushi Kosuge[6]

✉ Zeeshan Ahmed
zeeshan@g.ecc.u-tokyo.ac.jp

✉ Ravinder Kumar
ravinderkumar@g.ecc.u-tokyo.ac.jp

✉ Shuichiro Miwa
miwa@n.t.u-tokyo.ac.jp

[1] Nuclear Professional School, The University of Tokyo, 2-22 Shirane-Shirakata, Tokai-Mura, Ibaraki 319-1188, Japan

[2] Department of Nuclear Engineering and Management, The University of Tokyo, 7-3-1 Hongo, Bunkyo-ku, Tokyo 113-8656, Japan

[3] School of Mechanical Engineering (SMEC), Vellore Institute of Technology, Chennai, Tamil Nadu 600127, India

[4] Nuclear Science Research Institute, Japan Atomic Energy Agency (JAEA), 2-4 Shirakata, Tokai-Mura, Ibaraki 319-1195, Japan

[5] Institute of Engineering Innovation, The University of Tokyo, 7-3-1 Hongo, Bunkyo-Ku, Tokyo 113-8656, Japan

[6] Tsuruga Comprehensive Research and Development Center, Japan Atomic Energy Agency (JAEA), 65-20 Kizaki, Tsuruga-Shi, Fukui 914-8585, Japan